IEEE Access
Multidisciplinary | Rapid Review | Open Access Journal

Received 10 July 2024, accepted 12 August 2024, date of publication 22 August 2024, date of current version 10 September 2024.

Digital Object Identifier 10.1109/ACCESS.2024.3448368

RESEARCH ARTICLE

Rendering Fine Tactile Feedback With a Novel Hydraulic Actuation Method for Wearable Haptic Devices

DANIELE LEONARDIS, DOMENICO CHIARADIA, GIANCARLO SANTAMATO, CRISTIAN CAMARDELLA, AND ANTONIO FRISOLI, (Senior Member, IEEE)
Institute of Mechanical Intelligence, Scuola Superiore Sant'Anna, Ghezzano, 56010 Pisa, Italy

Corresponding author: Daniele Leonardis (daniele.leonardis@santannapisa.it)

This work was supported by the Social and hUman ceNtered XR (SUN) project through European Union's Horizon Europe Research and Innovation Program under Grant 101092612.

This work involved human subjects or animals in its research. Approval of all ethical and experimental procedures and protocols was granted by the Ethical Review Board of Scuola Superiore Sant'Anna under Application No. 152021, and performed in line with the Declaration of Helsinki.

ABSTRACT Tiny contact transients prove very informative for dexterous, fine manipulation, both in virtual environments and teleoperation. Yet, it is challenging to obtain such quality of the rendering in compact and highly wearable haptic devices. To this aim we propose a novel miniature hydraulic actuator, aiming at low-noise rendering of tiny tactile signals, fully enclosed in a fingertip haptic device. Its novelty is in the use of ferrofluidic sealings, embedded within a miniature linear electromagnetic motor. The solution has two main advantages: it shows no static friction, due to the magnetohydrodynamic levitation effect of the ferrofluid, and a noiseless hydraulic reduction. Besides, the hydraulic actuator enables the use of a soft and compliant interface for transmission of signals to the fingerpad tissues. We evaluate here a prototype of the actuator implemented in a compact and soft haptic thimble: the low-noise rendering capabilities are evaluated in experiments at the bench and through perception study. Then, in a simplified teleoperation setup, we match one-to-one the pressure rendered by the device with a sensitive pneumatic pressure sensor mounted on a robotic fingertip. Results show that haptic feedback alone (no vision) is able to improve results over the visual condition in terms of maximum exerted pressure.

INDEX TERMS Haptic feedback, tactile, wearable, hydraulic, ferrofluid, virtual, telemanipulation.

I. INTRODUCTION

Haptic rendering provides the user fundamental sensory information and consequently it is crucial for effective task execution during virtual manipulation or teleoperation. Particularly, in fine manipulation the most of the interaction is located at the fingertips, thus the design of wearable devices - such as gloves and thimbles - has to comply with strict constraints: wearability, lightweight, inter-finger interference, quality and variety of the feedback.

The associate editor coordinating the review of this manuscript and approving it for publication was Zheng H. Zhu.

Haptic rendering is an essential sensory pathway for manipulation in virtual manipulation and teleoperation, as it provides users with crucial sensory information involved in the task execution. In fine manipulation tasks, the majority of interaction occurs at the fingertips. Therefore, the design of wearable devices, such as gloves and thimbles, must adhere to stringent constraints, including wearability, lightweight construction, minimal inter-finger interference, high-quality and diverse feedback rendering.

The variety of tactile sensation and stimuli has led to the creation of numerous haptic devices, encompassing vibratory [1], contact orientation [2], contact force [3], area of

contact [4], tangential slip [5] tactile information. [6] offers a comprehensive review of portable and wearable haptic devices.

A. WIDE BANDWIDTH RENDERING IN WEARABLE HAPTICS

Prior studies aimed at optimizing the intensity and dynamics of the rendered stimuli, involving a trade-off between static force, bandwidth, and actuator size. Fingertip devices

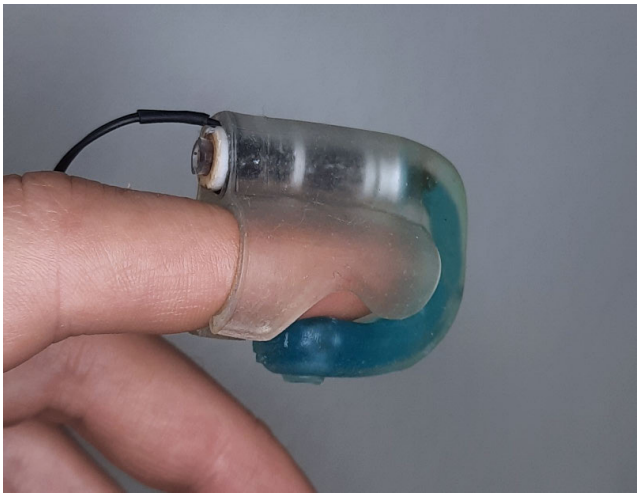

FIGURE 1. Prototype of the haptic thimble making use of the direct-drive hydraulic actuator.

employing direct-drive miniature electromagnetic actuators successfully achieve high-quality haptic rendering through a wide spectrum of signal frequencies. However, these devices come with the drawback of either limited maximum output force or considerable mass [7] for the fingertip application.

When these miniature actuators are coupled with gear reduction, the output force can be increased [2], [5], [8], [9] with a very limited mass increment. However, this comes at the expense of significantly reducing the output bandwidth and of introducing noise in the rendering. It is due to vibrations from the gears teeth and from friction generated by the transmission mechanism. To this regard it is important to consider the significance of transients and high-frequency components in the sense of touch, as reflected in the high sensitivity of fingerpad mechanoreceptors to fast dynamic signals [10]: this dynamic sensitivity is such that there is a frequency overlap between the tactile sensory channel and the auditory channel [11]. The perception of high-frequency signals proves crucial in texture perception [12] and tele-manipulation in general [13]. Additionally, there are factors impacting the quality of the haptic rendering, such as the presence of air gaps or excessive preloading forces between the device and the fingerpad. To this regard ergonomics of the interface and proper signal transmission between the actuated parts and the fingerpad tissues are of paramount importance.

B. PNEUMATIC AND HYDRAULIC HAPTIC INTERFACES

Pneumatic and hydraulic systems represent an interesting choice for haptic feedback, particularly when paired with soft surfaces interfacing the device to the fingerpad. Introducing

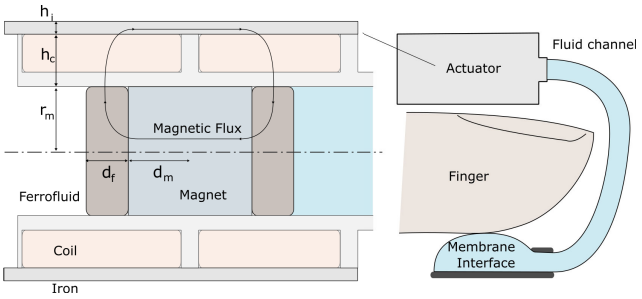

FIGURE 2. Scheme of the operation principle: the ferrofluid acts both as a frictionless hydraulic sealing and as a polar expansion for the electro-magnetic linear actuator.

inherent compliance in the interface has the potential of enhancing signal transmission, addressing the challenges associated with electromagnetic actuators, such as issues related to noise and non-linear behavior.

Examples of pneumatic actuation in wearable devices were presented in [14], [15], and [16] for rendering directional tactile signals to the wrist with a soft wearable interface. In the clinical field, a pneumatic multi-fingered actuator was proposed in [17] for remote palpation tasks. An interesting 4-dofs parallel soft structure, miniaturized for wearable application at the fingerpad, was presented in [18] and pneumatically actuated. The drawback of these designs is that usually pneumatic actuators require bulky units, positioned at a distance from the actuated body segment and connected to the wearable interface through tethers. To miniaturize such hydraulic actuators using conventional sealing methods (i.e rubber sealings and o-rings) would be difficult due to the significant increase of friction forces with respect to the actuation output forces. Moreover, conventional pumping mechanisms use cycled operation, that is not suitable for direct, linear modulation of the output signals.

A different technology makes use of low-boiling point liquids and thermal energy: thermo-pneumatic actuators can result in a very compact design, composed of just a sealed cavity filled with a low-boiling point liquid, and coupled with a heating element. Early investigation on this technology was performed for Braille or tactile display actuators [19], [20]; recently it has been proposed for wearable haptic devices [21]. Main limitations are in the output bandwidth, due to the need of fast energy absorption and dissipation in the liquid, especially when rendering dynamic signals. An innovative hydraulic actuator using electro-active-polymers in a stacked configuration has been proposed in [22] as a proof of concept for development as an haptic device.

Still, the quality of the signal can be affected if pressure modulation is pursued through conventional valves. In [23] a better performing actuating method was contrived to achieve accurate pressure modulation embedded in a

compact desktop device. In the work it is experimented with completely soft tethered silicone haptic thimbles. With the aim of rendering high-quality signals, [24] presented a different method for driving similar soft haptic thimbles with pneumatic pouches: in the study, remote audio speakers were sealed to tethers and in turn to the device, and used to linearly modulate pressure of the air chamber.

Inspired by the above methods, we investigated whether hydraulic or pneumatic actuators could be miniaturized and embedded close to the actuated location, resulting in wearable, untethered devices with a compliant and noiseless interface to transmit signals to the skin.

C. FERROFLUID ACTUATORS IN HAPTICS

When reducing the size of the actuators, one concern with pneumatic sealings is to obtain smooth movements, due to the non-linear scaling of the friction and output forces. In [25], [26] sealed mechanical couplings with no static friction were achieved through the use of ferrofluids - stable colloidal dispersions of ferromagnetic nanoparticles in mineral oil. Ferrofluid was also adopted in miniature and micro pumps, as in [27] or medical actuators, as in [28]. In these architectures, a permanent magnet guaranteed to hold the position of a ferrofluidic sealing layer, while external actuators were used to drive the mechanism. In [29], a ferrofluid-based electromagnetic haptic actuator was developed, using the change of the volume in the magnetic circuit gap and the ferrofluid itself, enclosed in a membrane, as a direct mean to convey haptic sensations. In the recent [30] the ferrofluid sealing method was embedded directly within the active element of the electromagnetic actuator. Here the magneto-hydrodynamic levitation method was used for obtaining oscillatory movement of moving part, in the scope of a miniaturized pump for an artificial heart application.

In haptics, the use of ferrofluid as a shape-modulated mean through an external magnetic field (rather than as a frictionless hydraulic sealing), has been also proposed to obtain spatially distributed cues (i.e. [31], [32], [33]).

In this work we applied the principle of magneto-hydrodynamic levitation for obtaining clean and linear pressure modulation in a direct-drive, miniaturized haptic thimble. The main advantages with respect to alternative methods are in the low-noise, no backlash rendering, due to both the direct drive and soft hydraulic interface adhering to the fingerpad. With respect to similar pneumatic or hydraulic devices, the approach allows an embedded, untethered hydraulic chamber and linear, wide bandwidth rendering features.

The final prototype with the embedded hydraulic actuator is shown in Figure 1, and a scheme of the working principle is pictured in Figure 2: it obtains a compliant and soft interface with the skin with clean and noiseless output rendering. Preliminary findings and the actuator prototype are presented in [34]. We further investigate here how tiny contact transients can be rendered by the novel device into an experimental finger-teleoperation setup, and how these tactile information can improve performance of the subjects in the proposed task.

The paper is organized as follows. In Sec. II we present an electromagnetic model of the direct-drive hydraulic actuator, and the design of a first prototype. Experimental evaluation is presented in Sec. III: characterization of the actuator is presented in Sec. III-A. Sec. III-B is devoted to a user study meant to investigate the capabilities of the proposed approach for fine haptic rendering. Lastly, in Sec. III-C we experimentally evaluate the method in a simplified teleoperation setup, focused on haptic rendering of fine contact transients. Conclusion are presented in Sec. IVk.

II. MODEL OF THE DIRECT-DRIVE PNEUMATIC HAPTIC ACTUATOR

An electro-magnetic model has been developed for dimensioning the actuator and to understand the scaling factors related to the output force, pressure and displacement.

The following section describes the developed physical model of the actuator, which considers the elctro-magnetic circuit and the output pressure. It can be used for dimensioning the actuator geometry, taking advantage of the hydraulic force scaling effect.

The nomenclature associated to the following equations is disclosed in Figure 2. The model is axial-symmetric (cylindrical magnet and actuator) and also symmetric for the two magnetic poles.

In the hypothesis that the magnetic flux Φ is ideally enclosed in the magnetic circuit, it is written *Equation* 1, where H_c is the coercivity of the magnetic material, and R the reluctance for each section of the magnetic circuit (magnet, ferromagnetic material, coils).

$$R_m\Phi + R_f\Phi + R_c\Phi = H_c d_m \tag{1}$$

$$\mu_m = \frac{B_r}{H_c} \tag{2}$$

$$B_m = \frac{B_r}{2} \tag{3}$$

NeFeBr magnets show a linear demagnetization curve. Hence the device can be designed so that the magnetic flux intensity B_m in the magnet is equal to half of the remanence point B_r in the magnet. This choice maximizes the magnetic energy in the air gap. Also, we assumed the flux section to be constant throughout the magnetic circuit. Thus the length of the ferrofluid polar expansion (d_f) is chosen in order to match the section area of the magnet (A_m) with the cylindrical surface of the polar expansions oriented toward the coils (A_c). The parameters (r_m, d_f, h_c) are shown in Figure 2.

$$A_m = A_c \longrightarrow r^2\pi = 2\pi r_m d_f \longrightarrow d_f = \frac{r_m}{2} \tag{4}$$

Assuming that $R_f \ll R_c$ in Equation 1, knowing that Φ is equal to B_m times the section area A_m and substituting from

Equation 3 we find:

$$\begin{aligned} R_m\Phi + R_c\Phi &= \frac{2H_c d_m}{B_r A_m} = \frac{2d_m}{\mu_r A_m} = 2R_m \\ R_c &= R_m \\ \frac{h_c}{\mu_0 A_c} &= \frac{d_m}{\mu_m A_m} \end{aligned} \tag{5}$$

The coil thickness (h_c) is found by substituting the above terms from Equation 4 and then from Equation 2 as follows:

$$h_c = \frac{\mu_0}{\mu_m} d_m = \frac{H_c \mu_0}{B_r} d_m \tag{6}$$

To model the output pressure, we find the Lorentz force:

$$F_m = B_c i_{coil} l_{coil} \longrightarrow F_m = B_c J V_{coil} \tag{7}$$

where F_m is the output force, B_c the intensity of the magnetic field in the coil volume, i_{coil} the current intensity, l_{coil} the length of one winding turn, J the current density per section area and V_{coil} is the volume of the winding (to be considered here only the segment crossed by the magnetic field). Considering as before a constant section of the magnetic circuit in Equation 4, B_c is found:

$$B_c = \frac{\Phi}{A_c} = \frac{\mu_m H_c}{2} \frac{A_m}{A_c} = \frac{\mu_0 H_c}{2} \tag{8}$$

With $h_c \ll r_m$, the volume of the coil immersed the magnetic field can be approximated as follows (substituting from Equation 4 and Equation 6):

$$V_{coil} = 2\pi r_m h_c d_f = \pi r_m^2 d_m \frac{\mu_0 H_c}{B_r} \tag{9}$$

We find then the output force F_m and the pressure in the liquid chamber:

$$\begin{aligned} F_m &= J \frac{(\mu_0 H_c)^2}{2B_r} \pi r_m^2 d_m \\ P &= J \frac{(\mu_0 H_c)^2}{2B_r} d_m \end{aligned} \tag{10}$$

The equation evidences how the output force is proportional to the volume of the magnet. The force constant of the actuator (output force to current intensity ratio) K_f is found by substituting in the last passage from Equation 4, Equation 6 and Equation 10:

$$K_f = \frac{F_m}{i_{coil}} = \frac{F_m N}{J h_c d_f} = N \mu_0 H_c \pi r_m \tag{11}$$

where N is the number of winding turns crossed by the magnetic field. Finally we find from Equation 11 the pressure constant K_p of the actuator:

$$K_p = \frac{F_m}{i_{coil}} = \frac{F_m N}{J h_c d_f} = \frac{N \mu_0 H_c \pi}{r_m} \tag{12}$$

The described physical model can be used for a preliminary design and parametrization of the actuator. Because of the moving magnet setup, the length d_m has to be chosen depending on the desired actuator stroke. Regarding electrical parameters, different section of the copper wire used in the windings can match the desired supply voltage with respect to current intensity. Independently from the wire section, the nominal current density J in the windings depends on thermal dissipation limit.

A. FEM ELECTROMAGNETIC SIMULATION

Based on the above model, and considering final dimensions of the device and practical approximations for the magnets armature, an actuator has been designed according to the parameters listed in Table 1.

The Finite-element-method (FEM) has been used to simulate the electromagnetic characteristics. An axisymmetric model has been implemented and simulated with FEMM Magnetics software. In particular, we were interested in simulating the output pressure characteristic with and without the external iron armature, and at different displacements of the internal moving magnet.

The mesh size was automatically generated with adaptive size for the air boundary region (Conforming Delaunay Triangulation method) and with maximum 0.2 *mm* size for the actuator parts. The final mesh contained 6616 nodes. Regarding the simulated materials, air was used for the boundary region and for the plastic parts supporting the coils. The magnet was simulated as a Neodymium (NdFeBr) N40 cylindrical bar magnet, polarized along the longitudinal axis. Ferrofluid regions at the poles were simulated with a non-linear BH curve with values obtained from [35]. The iron armature region was considered made of pure iron for the (a) and (c) conditions, and made of air for the (b) and (d) conditions. The copper coil regions were implemented in the FEA as part of a series circuit, with current flowing in opposite directions for phases A and B. The circuit was simulated with 60 turns for each coil, based on the number of turns achievable in the physical prototype given the available volume.

A set of simulations were run for each condition. The first aimed at estimating the current intensity to output pressure characteristic, with (a) and without (b) the iron armature. Increasing current intensity values in 0.1 A steps were used from 0.0 A to 1.0 A.

1) FEA RESULTS

The current intensity to output pressure characteristic showed a linear behavior in the simulated range due to magnetic field intensity well below the saturation point of the iron and ferrofluidic regions (maximum magnetic field intensity equal to 1.24 T in the magnet). Results are shown in Figure 3. Regarding the presence or absence of the iron armature, given the longitudinal proportions of the actuator the effect on the output force was reduced, as visible in Figure 3. Therefore, in the final prototype implementation, it has been chosen an iron-less design to further reduce the weight of the actuator.

Regarding the second FEA condition, it evaluated how the output pressure was influenced by the displacement of the magnet. The symmetric mid position of the magnet

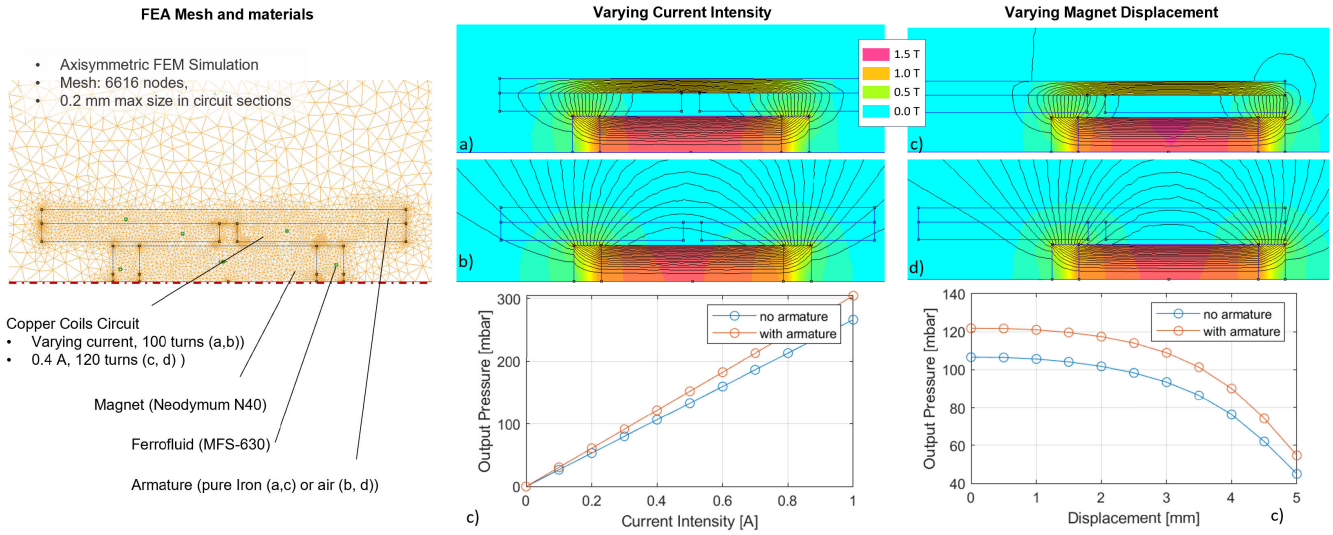

FIGURE 3. **FEM simulation: characteristic of the output pressure varying current intensity, and characteristic of the output pressure varying displacement of the moving magnet with respect to the center-line.**

maximizes the magnetic flux components in the coil regions perpendicular to the travel direction, hence obtaining the maximum output pressure (here simulated with 0.4 A constant current intensity). Conversely, during operation the magnet can be displaced from the mid position, reducing the output pressure. Simulation shows the output pressure drops at 90% of the maximum at ± 2.3 *mm* of travel, and at 50% of the maximum value at ± 4.7 *mm*, wich is at the limit of the designed stroke length (5 *mm*).

B. PROTOTYPE IMPLEMENTATION

The cylindrical body of the actuator was produced exploring two different methods: by SLA (stereolithography) 3D printing, and by CN manufacturing at the lathe from polyacetal (POM) plastic. The design constraint was the thickness of the coil support, which has to be the thinnest possible in order to minimize the air-gap in the magnetic circuit. Both manufacturing methods achieved good results. Also, the ferrofluid polar expansion allows for relaxing the required tolerance between the magnet and the inner diameter of the actuator body (here, 0.1 mm gap was used).

A collet was designed for the hydraulic connection between the actuator body and the soft thimble. On the other side, a mechanical end-stop at one end of the channel was added to prevent the magnet to slip away during assembly due to the absence of static friction.

To take full advantage from the hydraulic transmission solution, the whole thimble body was designed to be soft, with the actuator being the only rigid part, in order to improve the comfort and to better comply with different finger dimensions. To this purpose the shape of the thimble was designed with two flexible side flaps at the base of the finger phalanx. The hydraulic chamber was centered below the fingerpad and connected by a flexible channel to the actuator. The actuator was placed on the finger dorsum, outside the hand workspace. The thimble was designed with geometrical constraints such to allow printing in a single piece. SLA printing and flexible resin (Liqcreate Elastomer-X) were used. An overview of the parts implemented in the prototype is shown in Figure 4.

Concerning wearability of the device, the absence of actuators or rigid components in direct contact with the fingerpad contributed to improved comfort and fit of the soft thimble. The soft hydraulic chamber conformed effectively to the subjects' fingerpads without requiring additional adjustments, as experienced during the perception and teleoperation experiments described in the following sections.

On the other side, there are limitations in the current development and manufacturing methods to solve looking at the prolonged operation and robustness of the soft interface.

The soft resin material available nowadays for SLA printing proved permeable to liquids to some extent. In the time span of weeks or months, the liquid volume in the channel decreased, causing a change of the offset of the internal magnet. The resulting effect can be evaluated by the FEM simulation in the longitudinal displacement condition: within $\pm 2.3 mm$ of the magnet displacement, the output torque is still above 90% of the maximum value.

Additional investigation can be performed using different liquids (e.g., oils) or using coatings for the inner surfaces of the fluid channel the cavities. Other design constrains are due to the adopted 3D printing technique. Although SLA printing provides particularly good results when dealing with small features and details, the shape of the liquid channel must adhere to certain geometrical requirements in order to print the part in one piece. It has to be considered that soft resins are conversely more viscous than hard resins when uncured and

during printing. In order to clear uncured resin from the thin hydraulic channel, their section could not be reduced below $\sim 2mm$.

Finally, a mechanism to tune the volume of the chamber is to be considered for further developments and for extend compatibility of the device with different users. Although the soft structure of the thimble can already and comfortably accomodate different finger sizes, again the internal offset of the magnet will change, depending on the deformation at rest applied by the finger to the soft interface. A tuning mechanism can also optimize the amount of linear stroke designed for the internal magnet, which in turn determines the overall size of the actautor.

TABLE 1. Prototype parameters.

Parameter	Value	Unit
r_m	2	mm
d_m	4	mm
actuator length	22	mm
actuator mass	3.2	g
thimble total mass	7.8	g
R	6.8	Ω
K_p	0.2	bar/A
nominal voltage	3.7-5	V
nominal current	0.4	A
nominal pressure	75	mbar

C. FEM SIMULATION OF THE FINGERPAD INTERFACE

A FEM simulation has been performed to evaluate the deformation of the fingerpad interface. In the model, represented in Fig. 5(a), the finger was schematized including the bone and the cartilage, while the pouch was inflated with the nominal hydrostatic pressure equal to 75 mbar.

For the fingerbone material, we assumed a linear isotropic behavior with Young's modulus equal to 18 GPa, and a Poisson ratio equal to 0.2 which are the typical values adopted for the cancellous fingerbones [36], [37]. Instead, the soft tissue cartilage of the distal phalanx was modeled through a Neo-Hookean hyper-elastic material with constants $C_{10} = 0.34$ MPa and $D_{10} = 2.20$ MPa^{-1} [36], [38]. Lastly, an isotropic model was assumed for the pouch soft resin material with Young's modulus equal to 1.5 MPa and Poisson ratio equal to 0.49.

The overall domain was discretized with elements with a size of 1 mm and a linear order to preserve local instability effects. The contact between the pouch and the cartilage finger was simulated including a frictional behavior, admitting a frictional coefficient of 0.74 [37]. Due to the compliance of the finger cartilage and the resin pouch, a symmetric formulation was chosen for such a contact. The Augmented Lagrange method was adopted to achieve the most accurate contact results. Besides, a stabilization damping factor of 0.8 was necessary to dissipate the energy associated with the local instability of the mesh arising at the contact initiation. A fixed support constraint is imposed on the base of the finger and the pouch. Due to the high non-linearity of the problem, the solution was achieved by dividing the hydrostatic load into subsets. The true scale displacement contour is represented in the section view of Fig. 5(b). During inflation, the pouch experiences a large deformation, concentrated in the fingerpad region. In particular, sticking occurs, generating an ultimate contact area of 200 mm^2. Such a contact area behaves like a kinematic hinge for the pouch which rotates around the sticking area, achieving a maximum displacement of around 2.6 mm. At the same time, a gap is generated near the edge of the finger. No relevant deformation is visible outside the fingerpad region. On the other side, due to inflation, elastic stretch is concentrated in the thin wall region of the pouch, as shown in Fig. 5(c) where the equivalent Von Mises strain is represented.

In similar simulations, while the precise interaction forces might not represent a reliable estimation of the final device operation, due to different finger shapes and dynamically variable stiffness of the fingerpad tissues, the above results provide a qualitative evaluation regarding the area of deformation, which, as intended, is located at the middle of the fingerpad. Additional information to consider in further design is provided by the global displacement of the hydraulic pouch: increasing the stiffness of the structure connecting the pouch to the upper part of the thimble can reduce such compliance, and eventually increase deformation at the fingerpad. On the other hand, it would reduce the adaptability of the device to different finger sizes.

III. EXPERIMENTAL EVALUATION

Experimental characterization of the actuator was performed at the bench measuring the output characteristic, the step response and the dynamic bandwidth, both of the actuator only, and of the final prototype integrating the actuator in the soft thimble interface. Then, performance of the haptic thimble was evaluated in a perception experiment and through a simplified teleoperation scenario, exploring rendering of fine contact transients.

A. CHARACTERIZATION OF THE ACTUATOR

For the experimental characterization of the actuator, the hydraulic channel was connected through a silicone tube (4 mm internal diameter, 8 cm length) to an analog pressure sensor (MPXH6115AC6U) for measuring the output bandwidth, and to a digital pressure sensor (Bosch BMP280) for measuring the output pressure characteristic. A Teensy 3.6 microcontroller board and the Texas Instruments DRV8838 motor driver were used for acquiring the sensor data and for driving the actuator. The driver was powered by a 3.7V, 1200 mAh Li-Po battery. The current over pressure characteristic was estimated by driving the actuator with slow voltage ramps, both ascending and descending. The frequency response characterization was performed with a series of sinusoidal signals at different frequencies. The amplitude of the sinusoidal stimuli was equal to half the supply voltage. A second experimental characterization was performed to evaluate forces at the fingerpad applied by

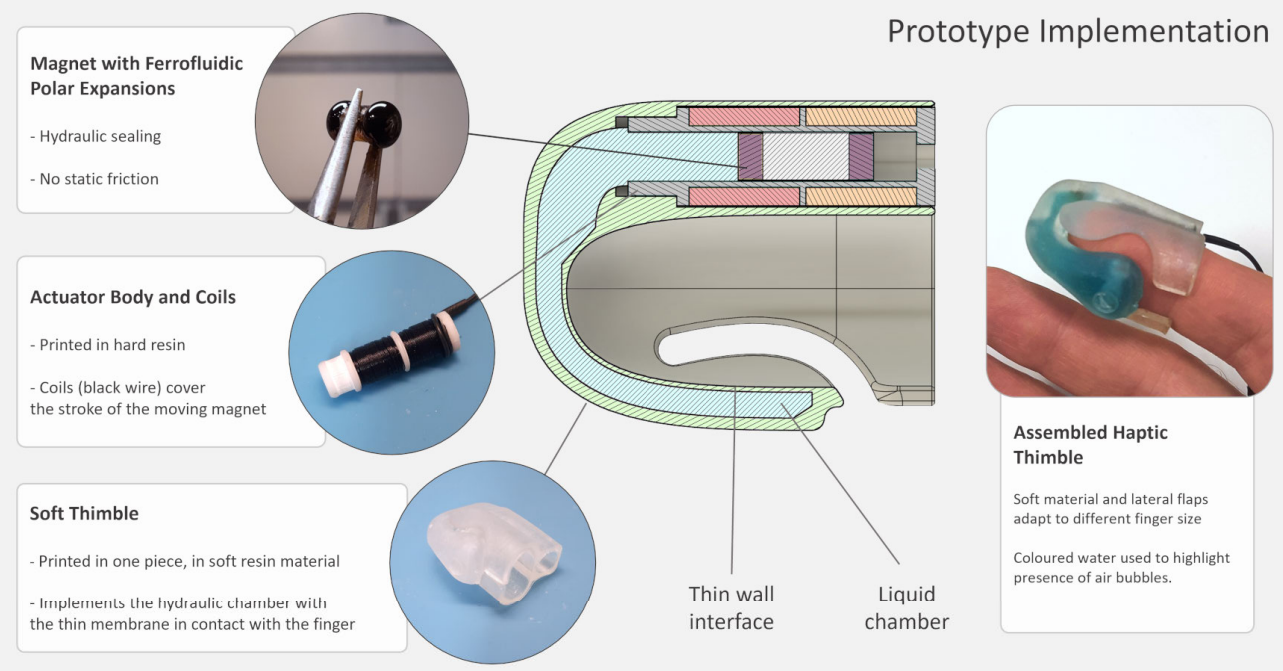

FIGURE 4. Overview and details of the prototype implementation.

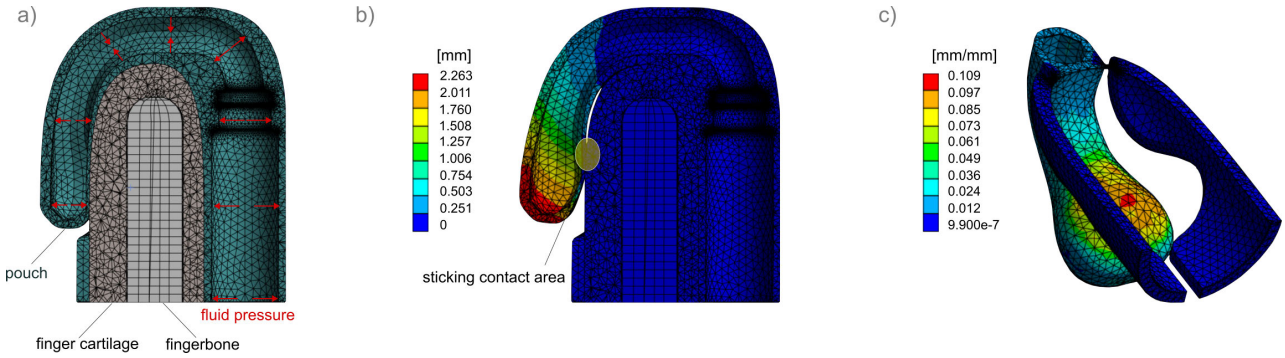

FIGURE 5. FEM simulation model. (a) Section view of the model, including the finger (bone and cartilage) and the fingerpad soft interface, with the pouch inflated at the nominal output pressure of the actuator. (b) Displacement contour plot showing the large deformation of the pouch and the effective contact area induced by the combined effect of inflation and frictional sticking. (c) Equivalent Von Mises strain contour plot: elastic stretch is concentrated in the contact area of the pouch.

the final fingertip device implementation (hence including the soft body, the liquid channel and the soft interface with the fingerpad). In the second experimental characterization including also the soft thimble, a miniature force sensor (OptoForce 10N, 2 mN resolution) was used, and mounted through a 3D printed support in the same position of the fingerpad (Figure 7).

1) CHARACTERIZATION RESULTS

The expected magneto-hydrodynamic effect of the ferrofluid polar expansions is highlighted by results of the characterization: Figure 6 (top) shows a linear characteristic, both in the loading and unloading direction, with no substantial static friction. The characteristic has been enlarged in the close-to-zero range to highlight how current values as low as 0.5% of the nominal range (corresponding to 3 mA) resulted in a measurable output pressure. Regarding the pressure constant of the actuator, the value of K_p is equal to 0.2 bar/A, which is 52% than the 0.38 value of the theoretical model. This result is closer with the current intensity to output pressure characteristic obtained in the FEM simulation (Figure 3), where the experimental value is 77% of the simulated value (0.26 bar/A for the condition without iron armature). The FEM simulation includes different non-ideal aspects the analytical model did not include. One is the magnetic flux not ideally confined within the modeled magnetic circuit, including also the direction of the flux not perpendicular to

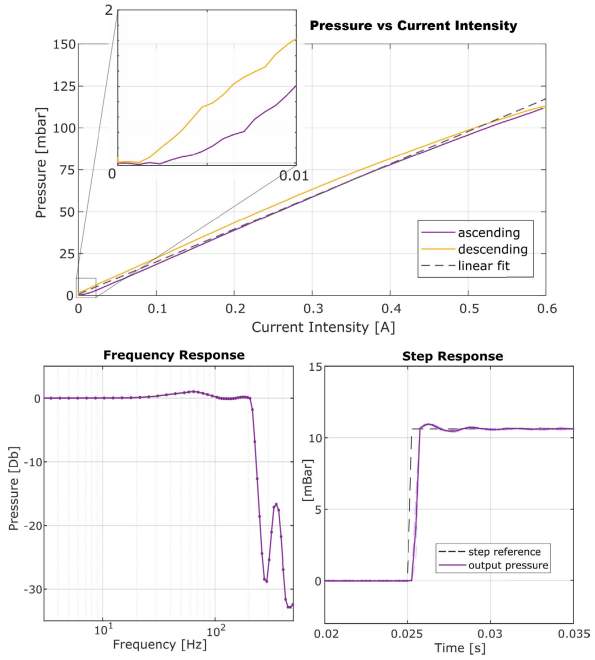

FIGURE 6. Characterization of the actuator at the bench: current intensity-to-output pressure characteristic (zoom in the Figure on the right highlights the substantial absence of static friction), frequency and step response.

the moving direction in the coils. Another relevant parameter is the actual number of the winding turns, given the volume of the coils: this value is difficult to estimate due the possibly uneven distribution of coil turns. The FEM simulation was set using a number of turns equal to the physical prototype.

Regarding the step response, results show a very repeatable behavior of the actuator. The signals, shown in Figure 6, are averaged over ten repetitions and reported with standard deviation lines (light dotted lines).

The measured output bandwidth of the actuator reaches the 200 Hz cut-off frequency. Such frequency response is particularly good when compared to the most of miniature actuators not specifically designed for wide-bandwidth haptic rendering. Conversely, voice coil and piezo actuators may surpass this value, although they face other constraints such as low-frequency rendering limit for piezo actuators, and relatively higher mass and encumbrance for voice coil devices.

Results of the second characterization session, using the force sensor at fingerpad (Figure 7) show the step response of the device including the liquid channel and the soft membrane in contact with the fingerpad (here, in contact with the force sensor). With respect to Figure 6, here the measured system includes the soft pouch and the contact distribution between the pouch and the hemispherical force sensor. According to the previous characterization, the reference step amplitude is set at the nominal current intensity of the actuator (0.4 A). The measured force amplitude of the step is 91 *mN* peak, 75 *mN* steady, as shown in Figure 6). Yet in this setup the measured force depends also on the area of contact between the soft interface and the sensor, which is more difficult to estimate. Regarding dynamic properties, the shape of the step

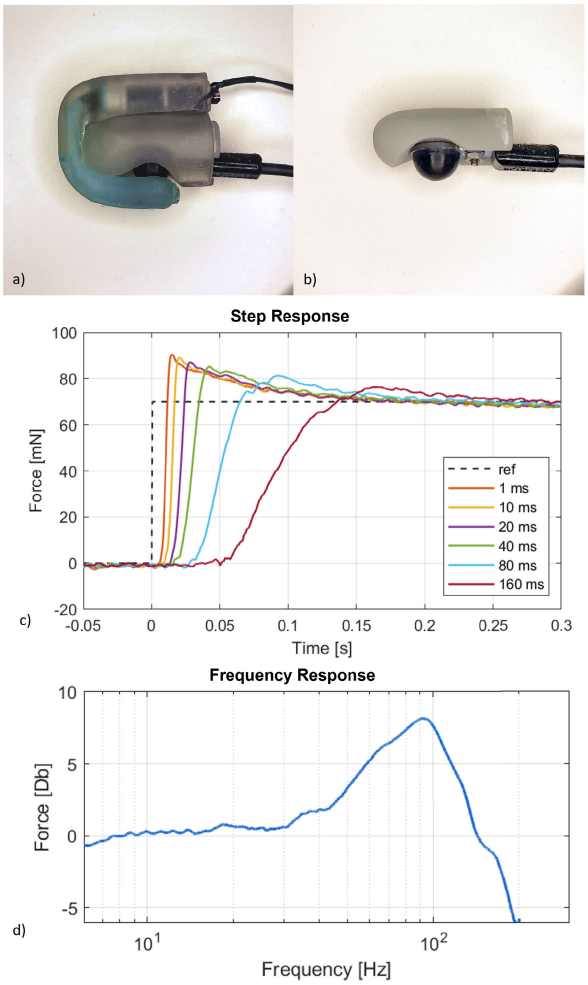

FIGURE 7. Characterization of the fingerpad interface using a miniaturized force sensor (a) in place of the finger (b). Step response with input amplitude equal to nominal current intensity of the actuator (0.4 A): comparison between sharp reference step response, and smoothed reference step responses as used in the perception experiment in Section III-B. (c) Frequency response.

response is different with respect to the sharp and highly repeatable step response of the actuator only, shown in 6. An overshoot is visible for the fastest step responses, and smoothed for the step responses using a slower sigmoidal rising edge as input. The presence of the overshoot, and the following decay toward the steady state amplitude, suggest the effect of the elastic and damping properties of the soft interface, excited by the higher frequency components of the sharp step input. We expect a similar elastic behavior to be present in other soft-interface actuators presented in literature, yet a direct comparison was not possible with the available characterization data.

The rise time, equal to 10 *ms*, is aligned with the measured frequency response shown in Figure 6. Here, the structure of the soft pouch introduces a resonating peak at about 92 Hz, and limits the output bandwidth to 175 Hz.

B. PERCEPTION EXPERIMENT

For the perception experiment, the final thimble prototype shown in Figure 1 was used. It aimed at measuring

minimum perception thresholds in discrimination of different contact transients. In the perception experiment and in the following teleoperation experiment, ten healthy subjects (aged from 25 to 40 years old, 7 male) were enrolled. The experimental procedures were approved by the Ethical Review Board of Scuola Superiore Sant'Anna (approval number 152021).

1) PERCEPTION EXPERIMENT SETUP

Two psychophysical perception experiments based on a forced-choice paradigm were performed. In both experiments, for each repetition a sequence of two stimuli was presented to the subject. The subject had to answer whether the perceived stimuli were equal or different. The stimuli were randomly chosen to be the same or different. A 3-down 1-up convergence method was used: for each wrong answer, the intensity of the stimuli (or difference from the sham stimuli) was increased (up step). Conversely the intensity of the stimuli was halved (down step) after a sequence of three correct answers. The first experiment used as stimuli two different raising edges, a pure step signal (sham stimulus) and a smoothed raising edge with sinusoidal shape (Figure 8 left). The intensity of the stimulus was set as the time length of the smoothed signal with respect to the sharp rising edge. By diminishing the length of the smoothed raising edge, the signal approaches the pure step sham stimulus. In the second experiment a similar smoothed rising edge stimuli was used and compared to a pure step sham stimuli. Here the intensity of the stimuli was modulated by the amplitude of both the signals, as shown in Figure 8 (left).

2) PERCEPTION EXPERIMENT RESULTS AND DISCUSSION

The first experimental condition investigated to what extent subjects were capable of discerning different rising edge shapes rendered by the proposed device in a simulated contact transient. Results show the sharp rising edge was distinguishable from the smoothed rising edge up to 54 ms length (Figure 8, right). Considering that the sense of touch spans to wider bandwidth limits [39], the result is meaningful of the device limits in rendering dynamic signals. The difference between the ideal step response and the generated sharp and smoothed step responses is clarified in Figure 7 (c). Due to the elastic and damping properties of the soft interface, a transient with an overshoot and a decay is visible. Also, the sharp step reference (marked as 1 ms) shows a rising time of $\sim$ 10 ms, attenuating the higher frequency components of the ideal response.

The second experimental condition investigated how the different contact transients were still distinguishable when diminishing the intensity of the transient. This is relevant also concerning haptic device design and implementation: miniature mechanism suffering non-linearities such as static friction or backlash may struggle to accurately render low-intensity signals, as seen, for instance, with miniature rotary motors with no ball bearings or in gear reducers. With the proposed device, the two reference signals could be distinguished up to 11 mbar intensity (mean value). To this regard, it has to be considered however that the hydraulic soft interface still introduces filtering in the rendered signal, as shown for the step response in the characterization of Figure 7. Convergence results are shown in Figure 8 (middle).

C. FINGER TELEOPERATION EXPERIMENT

The experiment aimed at exploring capabilities of the device in rendering fine contact thresholds in a real teleoperation setup, although simplified to a single dof.

1) TELEOPERATION EXPERIMENT SETUP

The teleoperation setup implemented a pressure-based sensorized finger, in order to match one to one the measured pressure with the rendered haptic signal. The sensor was built using a soft silicone dome with 8 mm axial radius and 24 mm length (Figure 9) and a pressure sensor (BOSCH BMP280). This method allows for a wide sensitive area, corresponding to the whole silicone dome surface. Sensitiveness can be adapted using different pressure sensors; here, for the implemented device the sensitivity was 0.12 *mBar* (equal to 1.2 mN for a 1 cm^2 contact area) which is relatively high compared to light object manipulation. The sensor was mounted on a robotic finger actuated by a servomotor (Feetech STS3215) with magnetic encoder at the output shaft and controlled with a position feedback loop.

At the leader side, the user was equipped with a custom made data-glove, implementing a bending sensor (73 mm length resistive bending sensor by SpectraSymbol) to measure the bending of the first phalanx. Sensor output was linearized between the open and closed (90° angle of the first phalanx) finger position. Overview of the teleoperation setup is shown in Figure 10.

Teleoperation loop was operated at 100 Hz, limited by the maximum sampling rate of the pressure sensor. Although higher rates are usually required for stability in force-feedback teleoperation, here the setup consisted of a tactile-feedback teleoperation, hence not subjected to stability issues. Subjects were asked to wear the data-glove and the haptic thimble, and seated in front of a desk in front of the teleoperated robotic finger. The experiment was performed in three conditions: with visual and haptic feedback (HV) with haptic feedback only (H) by covering the robotic finger with a panel, and with visual feedback only (V) by turning off the haptic rendering. In each condition, subjects were asked to repeatedly close the index finger up to reach the contact with a fixed finger opposed to the actuated robotic finger, then to stop and go back to the open hand position as soon as they perceived the contact (by vision or touch). In order to minimize motor memory, distance between the starting position and contact was randomly changed after each trial.

2) TELEOPERATION EXPERIMENT RESULTS AND DISCUSSION

Regarding the teleoperation experiment, the haptic only (no vision) condition is rarely performed in literature. Here it was possible due to the simplified single dof setup and to

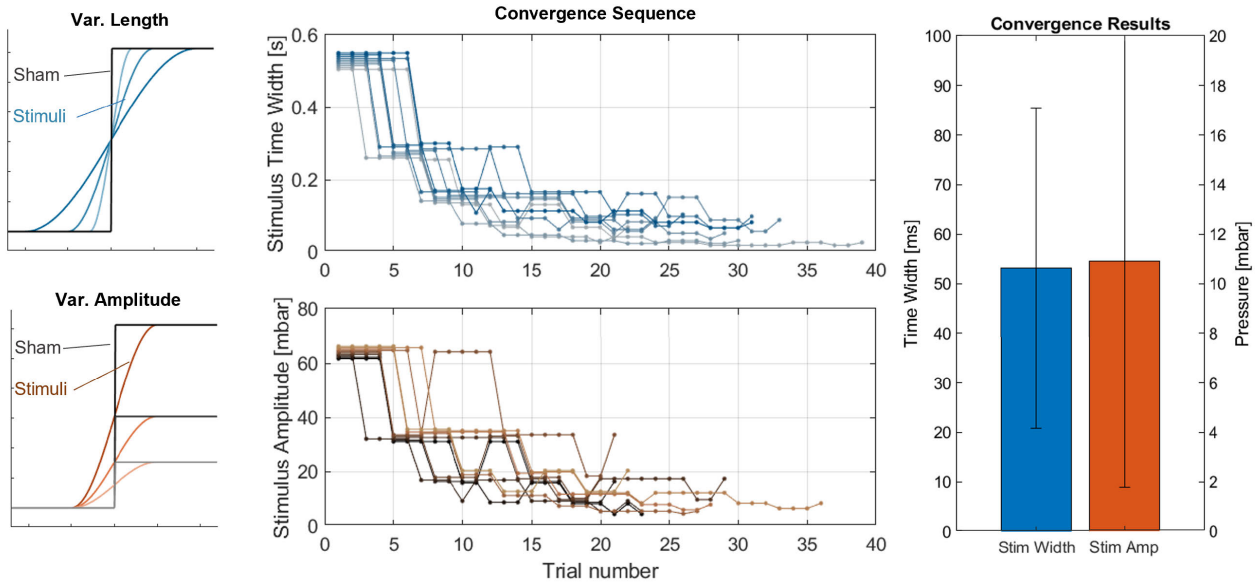

FIGURE 8. Psychophysical experiment: presented stimuli (left), convergence results (mid) and averaged perception thresholds (right).

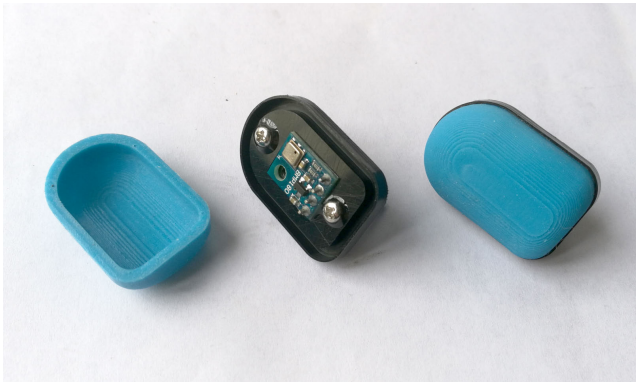

FIGURE 9. The sensitive fingerpad sensor developed for the robotic finger: a pressure sensor is embedded in a pressure chamber underneath a soft silicone dome.

the absence of more complex motor coordination. Noticeably, results of the H condition (Figure 11) significantly improved over the V for the exerted pressure and for the reference position indent, evidencing the consistency of the provided feedback. The HV condition performed very close to the H condition only for the pressure and indentation indices. Averaged values for the Contact Pressure are H: 26.7, HV: 28.7, V: 37.1 mbar with statistical significant differences between H and V ($p < 0.003$) and HV and V ($p < 0.019$). Averaged values for the Position Indent are H: 2.78, HV: 2.85, V: 3.22 mm with statistical significant differences between H and V ($p < 0.011$). Regarding velocity at the contact threshold (Contact Velocity) and time required to reach the contact condition (Time to Contact) the V and HV were performed with significantly higher velocities than the H. This is in agreement with the additional spatial information provided by vision, allowing to estimate the contact distance before reaching the contact condition. Subjects seem to have followed a more cautious strategy in approaching the contact threshold for the H. Averaged values for the Contact Velocity are H: 8.15, HV: 12.14, V: 15.96 mm/s with statistical significant differences between H and V ($p < 0.001$) and H and HV ($p < 0.016$). Averaged values for the Time to Contact are H: 4.29, HV: 3.20, V: 2.85 s with statistical significant differences between H and V ($p < 0.035$).

Interestingly, the HV did not perform the best in all the metrics, as it might be expected by the integration of the two different sensory modalities. The overall result for the HV can be explained considering the different task execution strategies adopted by subjects, and to the presence of two complementary metrics (contact intensity and speed). In the HV, the adopted strategy was probably to rapidly approach the target as in the V, and then to reduce the speed in proximity of the estimated contact position, in order to perceive the exact contact threshold by tactile feedback. Hence, the average contact velocity and execution time for the HV appears in between the V and H condition. Regarding the contact pressure and indentation metric, the averaged results appear very close between the H and HV with no significant difference, while both significantly different from the V. It suggests subjects were effectively using the provided tactile information also in the HV, with no additional benefits carried by vision in the precise perception of the contact threshold.

In Figure 11 (left) we show for a sample subject the behavior in the time domain of the contact condition. In agreement with the aggregated results, it can be noticed how the subject approached the contact threshold at different velocities depending on the sensory condition. Maximum values of the contact pressure shows how tiny transients could be precisely perceived also with haptic feedback alone, without visual guidance.

IV. CONCLUSION

In this work, we investigated how low-noise, tiny tactile stimuli can be rendered by wearable haptic devices. To this purpose, a novel miniaturized hydraulic actuator was devel-

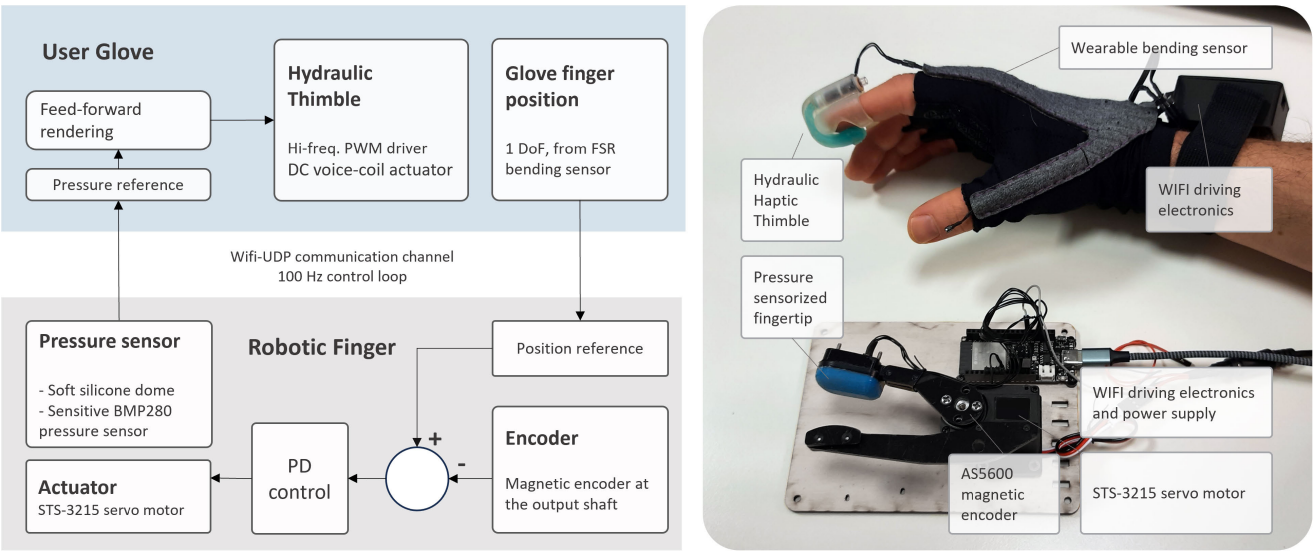

FIGURE 10. Setup of the simplified (single dof) teleoperation experiment, investigating perception of contact thresholds with a 1:1 match of the measured and rendered pressure.

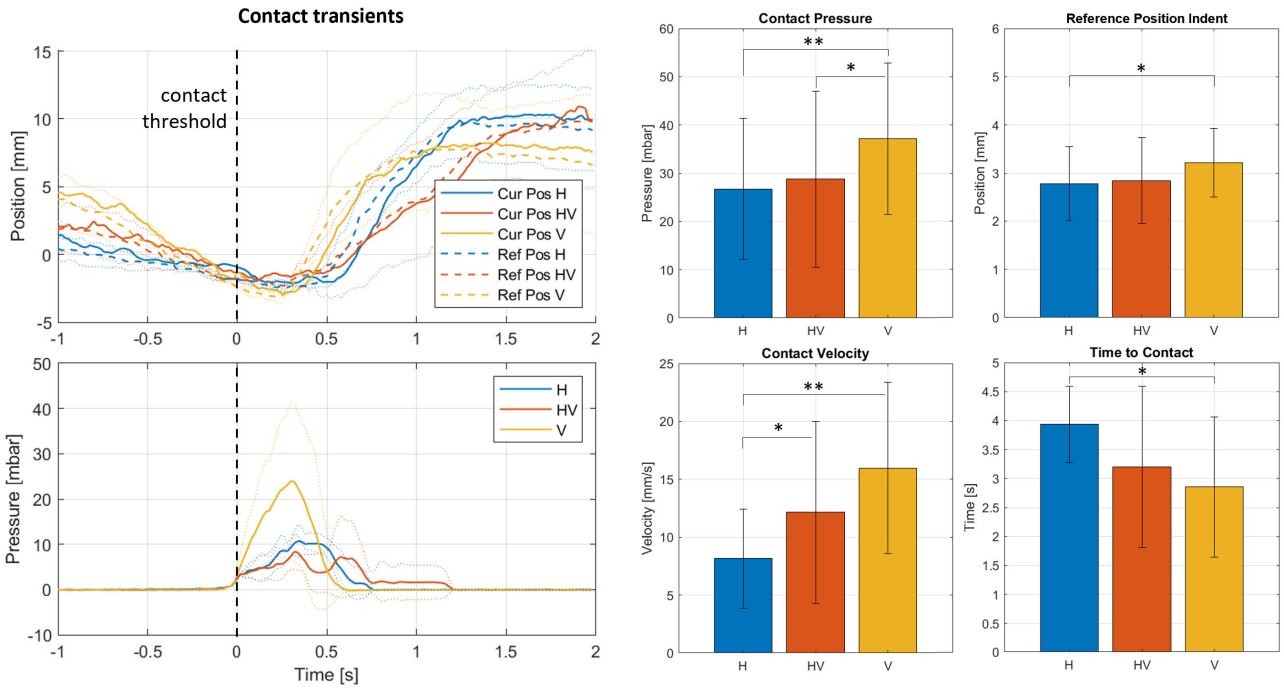

FIGURE 11. (left) Contact transients averaged over ten repetitions of a sample subject for the three experimental conditions. (right) Aggregated results of all subjects. The * and ** symbols represent a statistical significant difference with $p < 0.05$ and $p < 0.01$ respectively.

oped, showing a highly linear output due to the substantial absence of static friction. The effect was obtained using ferrofluid as hydraulic sealings and at the same time as polar expansions of a linear electromagnetic actuator. The method results in a direct drive, miniature hydraulic actuator, suitable for implementation in wearable haptics applications. With respect to other pneumatic solutions, the advantage is of being a miniature, self-enclosed actuator rather than tethered with remote pumps. With respect to other linear and wide bandwidth solutions such as piezo and voice-coils, the advantage is in the rendering capability extended to low dynamics and static signal for the first, and in lower encumbrance and soft interface for the latter. The use of flexible SLA resins allowed for a single-piece construction of the soft thimble, integrating the hydraulic chamber and a soft and compliant interface with the fingerpad. The whole soft thimble has been simulated with FEM, validating the main actuated area is located at the middle of the fingerpad.

The analytical model presented in this work is proposed for a first dimensioning step of a novel actuator design, while the conducted magnetic FEM analysis showed a closer matching with the final prototype characterization, due to modeling of non-ideal effects of the magnetic circuit. Characterization and perception results highlighted the interesting capability

in clean rendering of tiny transients, although the response deviated from the ideal one for the fastest dynamic stimuli, due to the compliance of the soft interface. This feature is difficult to achieve with conventional miniature actuators and is relevant for conveying contact information during fine manipulation tasks. The intensity and frequency content of discrete transients becomes informative of contact threshold with different velocities or with hard and soft materials [40], and of slip condition. Additional studies can be performed regarding the shape and stiffness of the soft fingerpad interface: here, a first characterization with a miniature force sensor in place of the finger was performed, evidencing a resonant peak and a more limited frequency bandwidth. However, such evaluation is challenging to perform especially in terms of intensity of the perceived signal, due to the difference between the real fingerpad, presenting a wider contact area and distribution of mechanoreceptors, and the force sensor, performing a lumped measurement of the signal intensity.

The conducted teleoperation experiment, although in a simplified single dof setup, evidenced interesting performance in fine modulation of a contact threshold with a 1:1 matching between the measured and rendered pressure. Remarkably, the maximum exerted pressure metric performed better in the haptic only condition (without vision).

While rendering performance were overall satisfactory and particularly good in terms of linearity and low noise of low amplitude signals, on the other side other design and usability aspects have to be addressed to reach full usability of the device in the long term. In particular, existing 3D printed soft resins appear permeable to liquids in the long term (weeks or months), changing the amount of liquid in the channel and therefore the offset of the magnet in the actuator. Further developments can involve both different materials (resin, liquid, or internal coating) to solve this issue, as well as a tuning mechanism for the volume of the actuated chamber. The latter in particular would allow also for a broader compatibility of the device for different finger sizes. Even if the structure of the thimble is soft, different finger sizes result in different offset position of the internal magnet at rest. Beyond the conceived full-device design implemented in this work, the core direct-drive hydraulic actuator can be potentially implemented to other hydraulic/pneumatic design, yet with remote tethered actuation, already proposed in literature, such as the 4 dofs soft device presented in [18]. More complex and ergonomic distribution of the soft interface at different locations of the hand can also be envisaged, exploiting the potential of the 3D printed soft structures.

REFERENCES

[1] M. Solazzi, A. Frisoli, and M. Bergamasco, "Design of a novel finger haptic interface for contact and orientation display," in *Proc. IEEE Haptics Symp.*, Mar. 2010, pp. 129–132.

[2] F. Chinello, M. Malvezzi, C. Pacchierotti, and D. Prattichizzo, "Design and development of a 3RRS wearable fingertip cutaneous device," in *Proc. IEEE Int. Conf. Adv. Intell. Mechatronics (AIM)*, Jul. 2015, pp. 293–298.

[3] D. Leonardis, M. Solazzi, I. Bortone, and A. Frisoli, "A wearable fingertip haptic device with 3 DoF asymmetric 3-RSR kinematics," in *Proc. IEEE World Haptics Conf. (WHC)*, Jun. 2015, pp. 388–393.

[4] S. Fani, S. Ciotti, E. Battaglia, A. Moscatelli, and M. Bianchi, "W-FYD: A wearable fabric-based display for haptic multi-cue delivery and tactile augmented reality," *IEEE Trans. Haptics*, vol. 11, no. 2, pp. 304–316, Apr. 2018.

[5] Y. Mo, A. Song, L. Zhu, Q. Ji, T. Wang, and H. Qin, "Design and evaluation of a wearable fingertip device for three-dimensional skin-slip display," *IEEE Trans. Haptics*, vol. 1, no. 1, pp. 1–8, Jul. 2024.

[6] C. Pacchierotti, S. Sinclair, M. Solazzi, A. Frisoli, V. Hayward, and D. Prattichizzo, "Wearable haptic systems for the fingertip and the hand: Taxonomy, review, and perspectives," *IEEE Trans. Haptics*, vol. 10, no. 4, pp. 580–600, Oct. 2017.

[7] M. Gabardi, M. Solazzi, D. Leonardis, and A. Frisoli, "A new wearable fingertip haptic interface for the rendering of virtual shapes and surface features," in *Proc. IEEE Haptics Symp. (HAPTICS)*, Apr. 2016, pp. 140–146.

[8] D. Leonardis, M. Solazzi, I. Bortone, and A. Frisoli, "A 3-RSR haptic wearable device for rendering fingertip contact forces," *IEEE Trans. Haptics*, vol. 10, no. 3, pp. 305–316, Jul. 2017.

[9] S. B. Schorr and A. M. Okamura, "Three-dimensional skin deformation as force substitution: Wearable device design and performance during haptic exploration of virtual environments," *IEEE Trans. Haptics*, vol. 10, no. 3, pp. 418–430, Jul. 2017.

[10] S. J. Bensmaia and M. Hollins, "Complex tactile waveform discrimination," *J. Acoust. Soc. Amer.*, vol. 108, no. 3, pp. 1236–1245, Sep. 2000.

[11] J. M. Yau, J. B. Olenczak, J. F. Dammann, and S. J. Bensmaia, "Temporal frequency channels are linked across audition and touch," *Current Biol.*, vol. 19, no. 7, pp. 561–566, Apr. 2009.

[12] M. Wiertlewski, J. Lozada, and V. Hayward, "The spatial spectrum of tangential skin displacement can encode tactual texture," *IEEE Trans. Robot.*, vol. 27, no. 3, pp. 461–472, Jun. 2011.

[13] K. J. Kuchenbecker, J. Gewirtz, W. McMahan, D. Standish, P. Martin, J. Bohren, P. J. Mendoza, and D. I. Lee, "Verrotouch: High-frequency acceleration feedback for telerobotic surgery," in *Proc. Int. Conf. Hum. Haptic Sens. Touch Enabled Comput. Appl.*, 2010, pp. 189–196.

[14] M. Raitor, J. M. Walker, A. M. Okamura, and H. Culbertson, "WRAP: Wearable, restricted-aperture pneumatics for haptic guidance," in *Proc. IEEE Int. Conf. Robot. Autom. (ICRA)*, May 2017, pp. 427–432.

[15] K. T. Yoshida, C. M. Nunez, S. R. Williams, A. M. Okamura, and M. Luo, "3-DoF wearable, pneumatic haptic device to deliver normal, shear, vibration, and torsion feedback," in *Proc. IEEE World Haptics Conf. (WHC)*, Jul. 2019, pp. 97–102.

[16] L. He, R. Wang, and X. Xu, "PneuFetch: Supporting blind and visually impaired people to fetch nearby objects via light haptic cues," in *Proc. Extended Abstr. CHI Conf. Human Factors Comput. Syst.*, Apr. 2020, pp. 1–9.

[17] M. Li, S. Luo, T. Nanayakkara, L. D. Seneviratne, P. Dasgupta, and K. Althoefer, "Multi-fingered haptic palpation using pneumatic feedback actuators," *Sens. Actuators A, Phys.*, vol. 218, pp. 132–141, Oct. 2014.

[18] Z. Zhakypov and A. M. Okamura, "FingerPrint: A 3-D printed soft monolithic 4-degree-of-freedom fingertip haptic device with embedded actuation," in *Proc. IEEE 5th Int. Conf. Soft Robot. (RoboSoft)*, Apr. 2022, pp. 938–944.

[19] F. Vidal-Verdú, M. J. Madueno, and R. Navas, "Thermopneumatic actuator for tactile displays and smart actuation circuitry," in *Smart Sensors, Actuators, and MEMS II*, vol. 5836. Bellingham, WA, USA: SPIE, 2005, pp. 484–492.

[20] H.-J. Kwon, S. W. Lee, and S. S. Lee, "Braille dot display module with a PDMS membrane driven by a thermopneumatic actuator," *Sens. Actuators A, Phys.*, vol. 154, no. 2, pp. 238–246, Sep. 2009.

[21] R. Uramune, H. Ishizuka, T. Hiraki, Y. Kawahara, S. Ikeda, and O. Oshiro, "HaPouch: A miniaturized, soft, and wearable haptic display device using a liquid-to-gas phase change actuator," *IEEE Access*, vol. 10, pp. 16830–16842, 2022.

[22] I.-D. Sirbu, D. Preninger, D. Danninger, L. Penkner, R. Schwödiauer, G. Moretti, N. Arnold, M. Fontana, and M. Kaltenbrunner, "Electrostatic actuators with constant force at low power loss using matched dielectrics," *Nature Electron.*, vol. 6, no. 11, pp. 888–899, Nov. 2023.

[23] B. J. Caasenbrood, F. E. van Beek, H. K. Chu, and I. A. Kuling, "A desktop-sized platform for real-time control applications of pneumatic soft robots," in *Proc. IEEE 5th Int. Conf. Soft Robot. (RoboSoft)*, Apr. 2022, pp. 217–223.

[24] Y.-L. Feng, R. L. Peiris, C. L. Fernando, and K. Minamizawa, "3D printed haptics: Creating pneumatic haptic display based on 3D printed airbags," in *Proc. Int. Conf. Human Haptic Sens. Touch Enabled Comput. Appl.*, 2018, pp. 180–192.

[25] I. Torres-Díaz and C. Rinaldi, "Recent progress in ferrofluids research: Novel applications of magnetically controllable and tunable fluids," *Soft Matter*, vol. 10, no. 43, pp. 8584–8602, 2014.
[26] M. Kole and S. Khandekar, "Engineering applications of ferrofluids: A review," *J. Magn. Magn. Mater.*, vol. 537, Nov. 2021, Art. no. 168222.
[27] M. De Volder and D. Reynaerts, "Development of a hybrid ferrofluid seal technology for miniature pneumatic and hydraulic actuators," *Sens. Actuators A, Phys.*, vol. 152, no. 2, pp. 234–240, Jun. 2009.
[28] B. Assadsangabi, S. M. Hashem Jayhooni, M. Short, H. Zeng, and K. Takahata, "Ferrofluid-enabled micro rotary-linear actuator for endoscopic three-dimensional imaging and spectroscopy," *Smart Mater. Struct.*, vol. 29, no. 1, Jan. 2020, Art. no. 015025.
[29] N. Kastor, B. Dandu, V. Bassari, G. Reardon, and Y. Visell, "Ferrofluid electromagnetic actuators for high-fidelity haptic feedback," *Sens. Actuators A, Phys.*, vol. 355, Jun. 2023, Art. no. 114252.
[30] Y. Matia, H. S. An, R. F. Shepherd, and N. Lazarus, "Magnetohydrodynamic levitation for high-performance flexible pumps," *Proc. Nat. Acad. Sci. USA*, vol. 119, no. 29, Jul. 2022, Art. no. e2203116119.
[31] S. Hashizume, K. Takazawa, A. Koike, and Y. Ochiai, "Cross-field haptics: Multiple direction haptics combined with magnetic and electrostatic fields," in *Proc. IEEE World Haptics Conf. (WHC)*, Jun. 2017, pp. 370–375.
[32] H. Singh, B. Suthar, S. Z. Mehdi, and J.-H. Ryu, "Ferro-fluid based portable fingertip haptic display and its preliminary experimental evaluation," in *Proc. IEEE Haptics Symp. (HAPTICS)*, Mar. 2018, pp. 14–19.
[33] C.-H. Kuo and S. Smith, "Mechanical feedback analysis of a ferrofluid-based module with 2D dynamic traveling waves for tactile display application," *Displays*, vol. 61, Jan. 2020, Art. no. 101926.
[34] D. Leonardis, D. Chiaradia, and A. Frisoli, "A miniature direct-drive hydraulic actuator for wearable haptic devices based on ferrofluid magnetohydrodynamic levitation," in *Proc. IEEE World Haptics Conf. (WHC)*, Jul. 2023, pp. 293–298.
[35] I.-J. Yang, S.-W. Song, D.-H. Kim, K.-S. Kim, and W.-H. Kim, "Improvement in torque density by ferrofluid injection into magnet tolerance of interior permanent magnet synchronous motor," *Energies*, vol. 14, no. 6, p. 1736, Mar. 2021.
[36] B. Faudot, J.-L. Milan, B. Goislard de Monsabert, T. Le Corroller, and L. Vigouroux, "Estimation of joint contact pressure in the index finger using a hybrid finite element musculoskeletal approach," *Comput. Methods Biomechanics Biomed. Eng.*, vol. 23, no. 15, pp. 1225–1235, Nov. 2020.
[37] Y. Wei, Z. Zou, G. Wei, L. Ren, and Z. Qian, "Subject-specific finite element modelling of the human hand complex: Muscle-driven simulations and experimental validation," *Ann. Biomed. Eng.*, vol. 48, no. 4, pp. 1181–1195, Apr. 2020.
[38] B. J. A. R. Tony and M. S. Alphin, "Finite element analysis to assess the biomechanical behavior of a finger model gripping handles with different diameters," *Biomed. Human Kinetics*, vol. 11, no. 1, pp. 69–79, Jan. 2019.
[39] S. J. Lederman and R. L. Klatzky, "Haptic perception: A tutorial," *Attention, Perception Psychophysics*, vol. 71, no. 7, pp. 1439–1459, Oct. 2009.
[40] H. Culbertson and K. J. Kuchenbecker, "Importance of matching physical friction, hardness, and texture in creating realistic haptic virtual surfaces," *IEEE Trans. Haptics*, vol. 10, no. 1, pp. 63–74, Jan. 2017.

DANIELE LEONARDIS received the M.Sc. degree in automation engineering from the Polytechnic University of Bari, in 2009, and the Ph.D. degree in perceptual robotics from Scuola Superiore Sant'Anna, in 2015. He is currently an Assistant Professor in mechanical engineering at Scuola Superiore Sant'Anna. He is a the principal investigator of local and European research projects in the field of fine haptic feedback coupled with immersive virtual reality and experimented in rehabilitation settings. His research interests include haptic feedback, telemanipulation, and wearable robotics applied to the clinical field.

DOMENICO CHIARADIA received the M.S. degree (Hons.) in control theory and automation engineering from the Polytechnic University of Bari, Italy, in 2014, and the Ph.D. degree in perceptual robotics from Scuola Superiore Sant'Anna, in 2018. He is currently an Assistant Professor of mechanical engineering (ING-IND/13) focusing on robotics at Sant'Anna School of Advanced Studies, Pisa, Italy. He leads the group developing flexible and portable exoskeletons, and soft exosuits in the human–robot interaction (HRI) research area. His current research interests include physical human–robot interaction, rigid and flexible exoskeletons and soft exosuits for assistance and rehabilitation, mechanical design and control of flexible joints, and haptic interfaces.

GIANCARLO SANTAMATO received the M.Sc. degree in mechanical engineering from the Polytechnic University of Bari, in 2014, and the Ph.D. degree in robotics and vibrations from Scuola Superiore Sant'Anna, in 2020. He is currently a Postdoctoral Researcher at Scuola Superiore Sant'Anna. His research interests include nonlinear dynamics, the structural health monitoring of complex infrastructures, and the modeling of mechatronic systems for robotics applications.

CRISTIAN CAMARDELLA received the master's degree from the Polytechnic of Bari, in 2017, and the Ph.D. degree in emerging digital technologies from Scuola Superiore Sant'Anna, in 2021. He is currently a Researcher with the Perceptual Robotics Laboratory, Mechanical Intelligence Institute, Scuola Superiore Sant'Anna. He is working on distributed haptic systems, predictive systems, robotic platforms in the rehabilitation robotics field, and immersive VR serious games. His research interests include machine learning and artificial intelligence, robotic exoskeletons and control strategies, muscle synergies, and serious game optimization.

ANTONIO FRISOLI (Senior Member, IEEE) is currently a Full Professor of engineering mechanics and robotics with Scuola Superiore Sant'Anna (SSSA), Italy, where he leads the Human Robot Interaction, Intelligence Mechanical Institute. He is currently responsible of the SSSA macronode of the Artes4.0 competence center on collaborative robotics. He is very active in technology transfer and open innovation. He has been the Co-Founder of two spin-off, such as Wearable Robotics srl and Next Generation Robotics srl. His research interests include the area of collaborative, rehabilitation and wearable robotics, exoskeletons, multimodal interaction and haptics, wearable devices, and virtual reality. He is an Associate Editor of *IEEE Robotics Automation Magazine* and covers several scientific and editorial roles in scientific societies, such as Eurohaptics and ICORR, international conferences, and journals.

Open Access funding provided by 'Scuola Superiore ''S.Anna'' di Studi Universitari e di Perfezionamento' within the CRUI CARE Agreement